Oxygen Nonstoichiometry and Ionic Conductivity of $Sr_3Fe_{2-x}Sc_xO_{7-\delta}$

Alexey A. Markov,[†] Mikhail V. Patrakeev,[†] Vladislav V. Kharton,*[,‡] Yevheniy V. Pivak,[‡] Ilia A. Leonidov,[†] and Viktor L. Kozhevnikov[†]

Institute of Solid State Chemistry, Ural Division of RAS, 91 Pervomayskaya Street, Ekaterinburg 620219, Russia, and Department of Ceramics and Glass Engineering, CICECO, University of Aveiro, 3810-193 Aveiro, Portugal

Received May 20, 2007. Revised Manuscript Received June 12, 2007

The substitution of scandium for iron in the Ruddlesden−Popper $Sr_3Fe_{2-x}Sc_xO_{7-\delta}$ ($x = 0-0.3$) system increases tetragonal unit-cell volume and oxygen nonstoichiometry and decreases partial p- and n-type electronic conductivities studied in the oxygen partial pressure range from 1×10^{-20} to 0.7 atm at 973−1223 K. The solubility of Sc^{3+} corresponds to approximately $x \approx 0.35$. The relatively low, temperature-activated hole mobility indicates a small-polaron mechanism of the electronic transport, as for undoped $Sr_3Fe_2O_{7-\delta}$. The atomistic computer simulations showed that major contribution to the ionic conductivity is provided by the oxygen sites surrounded by iron cations in the perovskite-type layers of $Sr_3(Fe,Sc)_2O_{7-\delta}$ structure, whereas stable ScO_6 octahedra are essentially excluded from the oxygen diffusion processes. Minimum migration energy, 0.9−1.4 eV, was found for nonlinear pathways formed by the apical O1 sites linking iron−oxygen polyhedra along the *c*-axis and equatorial O3 positions in the perovskite-type planes. The direct O3 → O3 jumps are characterized with higher energetic barrier, 1.5−2.2 eV. Because of the increasing concentration of vacant O3 sites induced by scandium doping, the apparent activation energy for oxygen−ionic transport decreases from about 2 eV, as observed for undoped strontium ferrite at 1123−1223 K, down to 0.95−1.15 eV for $Sr_3Fe_{2-x}Sc_xO_{7-\delta}$ ($x = 0.2-0.3$). As a result, the partial ionic conductivity of $Sr_3Fe_{1.7}Sc_{0.3}O_{7-\delta}$ at temperatures below 1000 K becomes higher than that in $Sr_3Fe_2O_{7-\delta}$.

1. Introduction

Oxide materials with oxygen−ionic and electronic transport have promising applications in high-temperature electrochemical devices, such as ceramic membranes for oxygen separation and partial oxidation of hydrocarbons, electrodes of solid oxide fuel cells (SOFCs), and sensors.[1−3] An attractive combination of properties important for these applications, namely, a relatively high mixed conductivity, moderate thermal and chemical expansion, and substantial stability in reducing atmospheres, is known for the Ruddlesden−Popper type strontium ferrite, $Sr_3Fe_2O_{7-\delta}$.[4−9] The intergrowth structure of this compound (Figure 1) is built of perovskite-like $(SrFeO_{3-\delta/2})_2$ and rock-salt SrO layers, and comprises three different anion positions.[4,9] At low temperatures, oxygen vacancies are predominantly located in the apical O1 sites (according to the site notation from ref 9). In these conditions, the most likely mechanism of the anion diffusion involves consecutive O3 → O1 → O3 jumps along the octahedra edges; the limiting factor is related to low concentration of the O3 vacancies available for anion transfer,

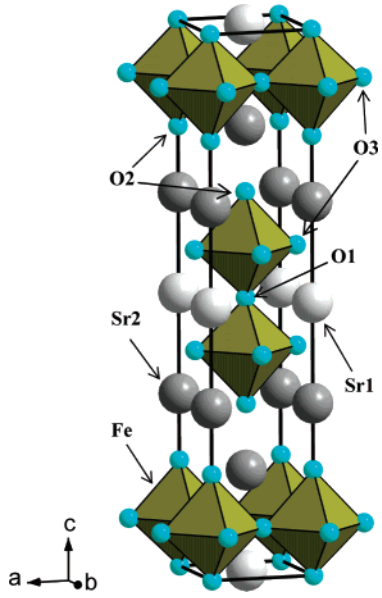

Figure 1. Crystal structure of $Sr_3Fe_2O_{7-\delta}$.

* Corresponding author. Tel: 351-234-370263. Fax: 351-234-425300. E-mail: kharton@ua.pt.
[†] Ural Division of RAS.
[‡] University of Aveiro.

(1) Brandon, N. P.; Skinner, S.; Steele, B. C. H. *Ann. Rev. Mater. Res.* **2003**, *33*, 183.
(2) Thursfield, A.; Metcalfe, I. S. *J. Mater. Chem.* **2004**, *14*, 2475.
(3) Ramirez-Salgado, J.; Fabry, P. *Sens. Actuators B* **2002**, *82*, 34.
(4) Dann, S. E.; Weller, M. T.; Currie, D. B. *J. Solid State Chem.* **1992**, *97*, 179.
(5) Shilova, Y. A.; Patrakeev, M. V.; Mitberg, E. B.; Leonidov, I. A.; Kozhevnikov, V. L. *J. Solid State Chem.* **2002**, *168*, 275.
(6) Patrakeev, M. V.; Leonidov, I. A.; Kozhevnikov, V. L.; Kharton, V. V. *Solid State Sci.* **2004**, *6*, 907.
(7) Mogni, L.; Fouletier, J.; Prado, F.; Caneiro, A. *J. Solid State Chem.* **2005**, *178*, 2715.
(8) Rakshit, S. K.; Parida, S. C.; Dash, S.; Singh, Z.; Sen, B. K.; Venugopal, V. *J. Solid State Chem.* **2007**, *180*, 523.
(9) Prado, F.; Mogni, L.; Cuello, G. J.; Caneiro, A. *Solid State Ionics* **2007**, *178*, 77.

10.1021/cm071364u CCC: $37.00
Published on Web 07/17/2007

governed by thermal fluctuations.[5,6] Increasing temperature promotes disordering in the oxygen sublattice of $Sr_3Fe_2O_{7-\delta}$, leading to vacancy redistribution between the O1 and O3 sites.[9] Consequently, the ion migration mechanism starts to change above 1100 K, probably indicating an increasing role of the O3−O3 pathway.[5,6,9] As oxygen diffusion in the Ruddlesden−Popper (RP) lattice is essentially two-dimensional, the ionic conductivity of $Sr_3Fe_2O_{7-\delta}$ is lower than that of perovskite-type $SrFeO_{3-\delta}$.[6] Nonetheless, these phases exhibit qualitatively similar behavior on doping, particularly because of the presence of similar structural elements in the Ruddlesden−Popper ($A_3B_2O_7$) and perovskite (ABO_3) compounds. For instance, incorporation of Ti^{4+} cations in the iron sublattice of $Sr_3Fe_2O_{7-\delta}$ was found to decrease oxygen deficiency and ionic conduction;[5] the effects of cobalt and nickel doping are opposite.[10] Analogous tendencies are well-known for the perovskite-type ferrite systems1[1−13].

The present work is focused on the study of oxygen nonstoichiometry and transport properties of Sc-substituted $Sr_3Fe_2O_{7-\delta}$. This type of doping was expected to increase oxygen deficiency, at least under oxidizing conditions when the average oxidation state of iron cations in $Sr_3Fe_2O_{7-\delta}$ is higher than 3+.[5−7] Moreover, doping of perovskite-type ferrites with stable trivalent cations, such as Sc^{3+}, Ga^{3+}, or Al^{3+}, leads usually to shifting redox equilibria toward lower oxidation states of iron.[14−17] The resultant increase in the oxygen-vacancy concentration may have a positive influence on the ionic conductivity. Another important factor is a strong preference of Sc^{3+} cations to octahedral oxygen coordination, which may further decrease the iron coordination numbers and, thus, may promote vacancy redistribution between the O1 and O3 sites in the $Sr_3Fe_2O_{7-\delta}$ lattice. To evaluate the relevance of these mechanisms to the ionic transport processes in $Sr_3Fe_2O_{7-\delta}$, atomistic computer simulations were performed.

2. Experimental Section

$Sr_3Fe_{2-x}Sc_xO_{7-\delta}$ ($x = 0.1-0.4$) were synthesized by solid-state reaction from the stoichiometric amounts of high-purity $SrCO_3$, Fe_2O_3, and Sc_2O_3, which was previously annealed in air at 1173 K to remove adsorbates. The reaction was conducted in air in the temperature range 1273−1573 K for 30−40 h with 4−5 intermediate grindings. Ceramics with density higher than 90% of the theoretical value were obtained after pressing to 200−300 MPa and sintering in air at 1623 K for 10 h. The processing conditions of undoped $Sr_3Fe_2O_{7-\delta}$ ceramics were reported in previous works.[5,6] Characterization of the materials included X-ray diffraction (XRD), pycnometry, and measurements of the oxygen content and total conductivity (4-probe DC) as a function of the oxygen partial pressure and temperature; experimental procedures and equipment were described elsewhere.[5,6,12,14−18]

Table 1. Comparison of the Experimental[a] and Calculated Unit-Cell Parameters of $Sr_3Fe_2O_{7-\delta}$

composition	lattice parameter	experimental	calcd	difference (%)
$Sr_3Fe_2O_7$	*a*	3.8526	3.8704	0.46
	c	20.1490	20.2806	0.65
$Sr_3Fe_2O_{6.5}$	*a*	3.8680	3.9210	1.35
	c	20.1582	20.7135	2.68
$Sr_3Fe_2O_6$	*a*	3.8940	3.9241	0.77
	c	20.0396	20.7632	3.49

[a] The experimental values are taken from ref 4 for $\delta = 0$ and 1.0, and from ref 22 for $\delta = 0.5$.

The static-lattice computer simulation studies based on the Born model for ionic solids were performed using the GULP software.[19,20] The modeling procedures were similar to those used for defect formation and migration processes in oxygen-deficient perovskite ferrites.[17,18] For this method, the ion charges determining long-range Coulombic forces are considered equal to the formal oxidation states (e.g., +3e for Fe^{3+}); the short-range interactions between *i* and *j* ions are described by the Pauli repulsion and van der Vaals dispersion models, expressed by the standard Bukingham potential (V_{ij})

$$V_{ij} = A_{ij}\exp\left(-\frac{r}{\rho_{ij}}\right) - C_{ij}r^{-6} \quad (1)$$

where r is the radius vector of a given ion, and A_{ij}, ρ_{ij}, and C_{ij} are parameters of the ion−ion interactions. The interatomic potential parameters and the properties of ions were obtained from the literature[18,21] and references cited therein; for Fe^{4+} cations, these parameters were taken from ref 17. The simulations of point defects, based on the Mott−Littleton approach, were carried out using a supercell consisting of 370 atoms. As the calculations are focused on the differences in vacancy formation and migration energies in various oxygen sites of nonstoichiometric strontium ferrite, the overall compositions were selected as $Sr_3Fe_2O_7$, $Sr_3Fe_2O_{6.5}$, and $Sr_3Fe_2O_6$. In the two latter cases, all oxygen vacancies were initially placed in the O1 positions, in accordance with structural data;[4,9] energetic effects caused by placing one vacancy in the occupied oxygen sites were then calculated. The potential cutoff radius and the region of most precise similations (so-called region 1) were selected as 12 and 10 Å, respectively. The simulated lattice parameters of $Sr_3Fe_2O_7$, $Sr_3Fe_2O_{6.5}$, and $Sr_3Fe_2O_6$ (Table 1) are all in a good agreement with experimental values,[4,22] although the difference between calculated and experimental values tends to increase with oxygen nonstoichiometry. The latter trend may be associated with an increasing role of vacant O3 sites when δ increases, in accordance with neutron diffraction data[9] and defect formation energies discussed below. As for the unit-cell parameters, the difference between experimental[4,22] and calculated bond-length values was lower than 1, 3, and 4% for $Sr_3Fe_2O_7$, $Sr_3Fe_2O_{6.5}$, and $Sr_3Fe_2O_6$, respectively.

(10) Mogni, L.; Prado, F.; Caneiro, A.; Manthiram, A. *Solid State Ionics* **2006**, *177*, 1807.
(11) Liu, Y.; Tan, X.; Li, K. *Catal. Rev.* **2006**, *48*, 145.
(12) Kharton, V. V.; Kovalevsky, A. V.; Tsipis, E. V.; Viskup, A. P.; Naumovich, E. N.; Jurado, J. R.; Frade, J. R. *J. Solid State Electrochem.* **2002**, *7*, 30.
(13) Wiik, K.; Aasland, S.; Hansen, H. L.; Tangen, I. L.; Odegard, R. *Solid State Ionics* **2002**, *152−153*, 675.
(14) Patrakeev, M. V.; Mitberg, E. B.; Lakhtin, A. A.; Leonidov, I. A.; Kozhevnikov, V. L.; Kharton, V. V.; Avdeev, M.; Marques, F. M. B. *J. Solid State Chem.* **2002**, *167*, 203.
(15) Patrakeev, M. V.; Markov, A. A.; Leonidov, I. A.; Kozhevnikov, V. L.; Kharton, V. V. *Solid State Ionics* **2006**, *177*, 1757.
(16) Kharton, V. V.; Waerenborgh, J. C.; Viskup, A. P.; Yakovlev, S. O.; Patrakeev, M. V.; Gaczyński, P.; Marozau, I. P.; Yaremchenko, A. A.; Shaula, A. L.; Samakhval, V. V. *J. Solid State Chem.* **2006**, *179*, 1273.
(17) Patrakeev, M. V.; Kharton, V. V.; Bakhteeva, Yu.A.; Shaula, A. L.; Leonidov, I. A.; Kozhevnikov, V. L.; Naumovich, E. N.; Yaremchenko, A. A.; Marques, F. M. B. *Solid State Sci.* **2006**, *8*, 476.
(18) Naumovich, E. N.; Patrakeev, M. V.; Kharton, V. V.; Islam, M. S.; Yaremchenko, A. A.; Frade, J. R.; Marques, F. M. B. *Solid State Ionics* **2006**, *177*, 457.
(19) Gale, J. d.; Rohl, A. L. *Mol. Simul.* **2003**, *29*, 291.
(20) Islam, M. S. *J. Mater. Chem.* **2000**, *10*, 1027.
(21) Freeman, G. M.; Catlow, V. R. A. *J. Solid State Chem.* **1995**, *85*, 65.
(22) Prado, F.; Armstrong, T.; Caneiro, A.; Manthiram, A. *J. Electrochem. Soc.* **2001**, *148*, J7.

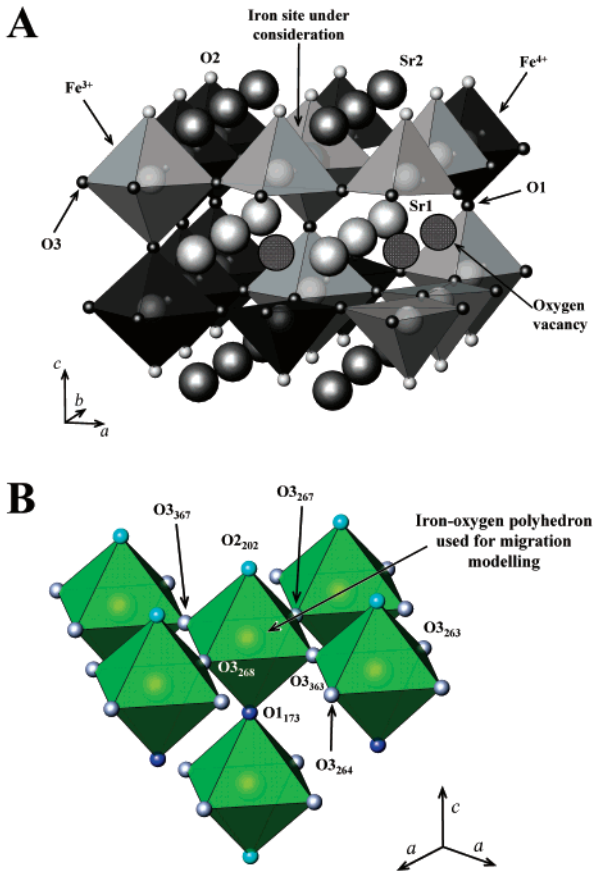

Figure 2. Point defect configuration near the central metal−oxygen octahedron used for modeling of the vacancy formation and migration processes in $Sr_3(Fe,Sc)_2O_{7-\delta}$ (A), and labeling of the corresponding oxygen sites (B).

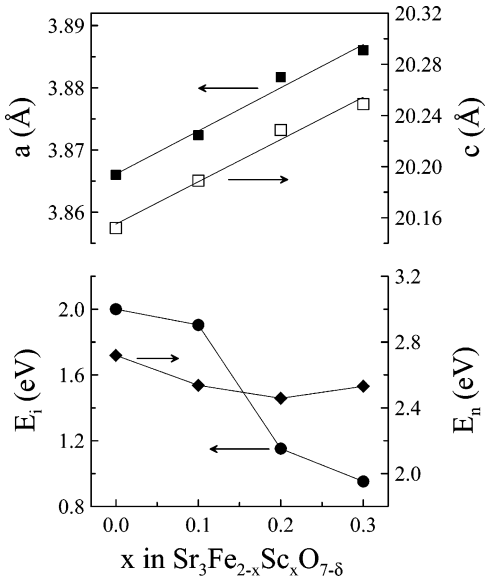

Figure 3. Room-temperature unit-cell parameters, apparent activation energy for the oxygen-ionic conductivity (E_i), and activation energy for n-type electronic conduction at $p(O_2) = 1 \times 10^{-16}$ atm (E_n) for the $Sr_3Fe_{2-x}Sc_xO_{7-\delta}$ series. The ionic conductivity activation energy of $Sr_3Fe_2O_{7-\delta}$ is given for the high-temperature range (see text).

For $Sr_3Fe_2O_{6.5}$, the initial distribution of Fe^{4+} cations and vacant O1 sites was random. To assess effects of scandium doping, we substituted one central Fe^{3+} ion in the $Sr_3Fe_2O_{6.5}$ supercell with Sc^{3+}; the resultant overall composition in this case is $Sr_3Fe_{1.97}Sc_{0.03}O_{6.5}$. Preliminary estimations demonstrated, however, that the

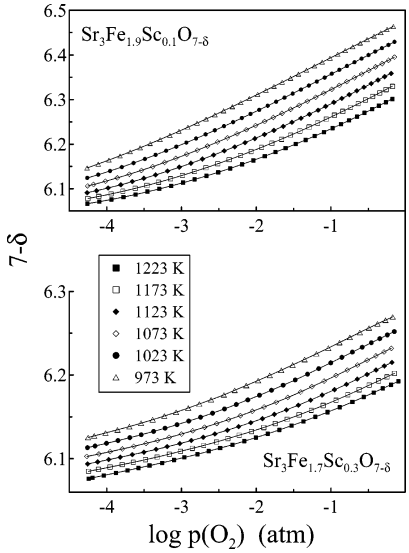

Figure 4. The $p(O_2)-T-\delta$ diagrams of $Sr_3Fe_{2-x}Sc_xO_{7-\delta}$ under oxidizing conditions, determined by the coulometric titration technique. Solid lines are for visual guidance only.

vacancy formation and migration energies depend substantially on surrounding defect configurations. Therefore, at the second stage of simulations, location of all ions in the corresponding crystallographic positions near Sc^{3+} was fixed, thus preserving local point-defect configurations; various oxygen sites with different neighborhoods were then tested. Consequently, the same defect configurations and oxygen sites were then examined for undoped $Sr_3Fe_2O_{6.5}$, with the central iron position occupied by Fe^{3+}. The local zone in the vicinity of this Sc^{3+}/Fe^{3+} position is shown in Figure 2A.

The energetic nonequivalence of oxygen sites with different point-defect neighborhood, which significantly affects the vacancy-formation energies, also leads to a significant difference of the migration energies (E_m) between crystallographically equivalent sites in $Sr_3(Fe,Sc)_2O_{7-\delta}$. In addition, an asymmetry of energetic barriers for the ion jumps was often observed. This makes it necessary to label atomic positions in order to distinguish particular pathways. In the present work, the sites are labeled according to the GULP indexing[19] for stoichiometric strontium ferrite. Figure 2B displays selected atomic indices for the central part of the supercell, relevant to the modeling results summarized below.

3. Results and Discussion

3.1. Structure, Oxygen Nonstoichiometry, and Total Conductivity: General Trends. XRD analysis showed that the solubility of scandium in $Sr_3Fe_{2-x}Sc_xO_{7-\delta}$ system corresponds to $x \approx 0.35$. The powders and ceramics with $x = 0.1-0.3$ were single phase; their structure was identified as tetragonal (S.G. I4/*mmm*), as for undoped $Sr_3Fe_2O_{7-\delta}$.[4,9,23] For $x = 0.4$, several impurity peaks corresponding to SrO and $Sr_4(Fe,Sc)_3O_{10-\gamma}$ solid solution were observed in the XRD patterns. The unit cell parameters of $Sr_3Fe_{2-x}Sc_xO_{7-\delta}$ increase with scandium content (Figure 3), primarily due to the larger size of Sc^{3+} compared to $Fe^{3+/4+}$.[24] One additional factor contributing to the lattice expansion relates to increasing oxygen deficiency on doping (Figure 4). The latter is

(23) Mori, K.; Kamiyama, T.; Kobayashi, H.; Torii, S.; Izumi, F.; Asano, H. *J. Phys. Chem. Solids* **1999**, *60*, 1443.
(24) Shannon, R. D. *Acta Crystallogr., Sect. A* **1976**, *32*, 751.

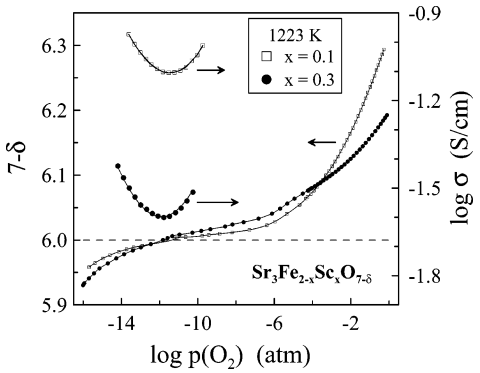

Figure 5. Oxygen nonstoichiometry variations in $Sr_3Fe_{2-x}Sc_xO_{7-\delta}$ within the studied $p(O_2)$ range. The total conductivity variations in the vicinity of electron−hole equilibrium points are shown for comparison. The solid lines plotted on the conductivity data points correspond to the fitting results (see text).

associated with decreasing oxidation state and thus increasing average radius of iron cations; similar tendencies are well-known for $SrFeO_3$-based perovskites substituted with Al^{3+}, Ga^{3+}, and Sc^{3+}.[14−17]

Figure 5 displays representative examples of the oxygen content variations in $Sr_3Fe_{2-x}Sc_xO_{7-\delta}$, for the whole $p(O_2)$ range where the RP phases exist at 1223 K. Again, the observed trends are typical for $Sr_3Fe_2O_7$- and $SrFeO_3$-based solid solutions.[5,6,14−17,25] Under oxidizing conditions, reducing $p(O_2)$ leads to extensive oxygen losses. The nonstoichiometry changes tend to approach a minimum level at $\delta \rightarrow 1$, when the average oxidation state of iron becomes 3+, and increase on further reduction. The plateaulike behavior in moderately reducing atmospheres corresponds to the so-called electron−hole equilibrium points, where the partial p-type and n-type electronic conductivities are equal. This is reflected by the characteristic minima in the total conductivity (σ) vs $p(O_2)$ isotherms, Figure 5. As the oxygen nonstoichiometry variations around these points are relatively small, the ionic conductivity (σ_i) in these conditions is essentially $p(O_2)$-independent, whereas the concentrations of p- and n-type electronic charge carriers can be considered proportional to $p(O_2)^{1/4}$ and $p(O_2)^{-1/4}$, respectively.[6,14,25,26] Consequently, the total conductivity variations can be approximated by the classical model[27,28]

$$\sigma = \sigma_i + \sigma_n^0 \cdot p(O_2)^{-1/4} + \sigma_p^0 \cdot p(O_2)^{1/4} \qquad (2)$$

where σ_n^0 and σ_p^0 are the values of partial n- and p-type electronic conductivities at unit oxygen pressure. The fitting results using this model, shown by solid lines in Figure 6, are in excellent agreement with experimental results; the minor deviations originate from slight changes in the oxygen vacancy concentration and ionic conductivity on reduction.

3.2. Oxygen Thermodynamics. The $p(O_2)$−T−δ diagrams of $Sr_3Fe_{2-x}Sc_xO_{7-\delta}$ (Figure 4) were used to calculate

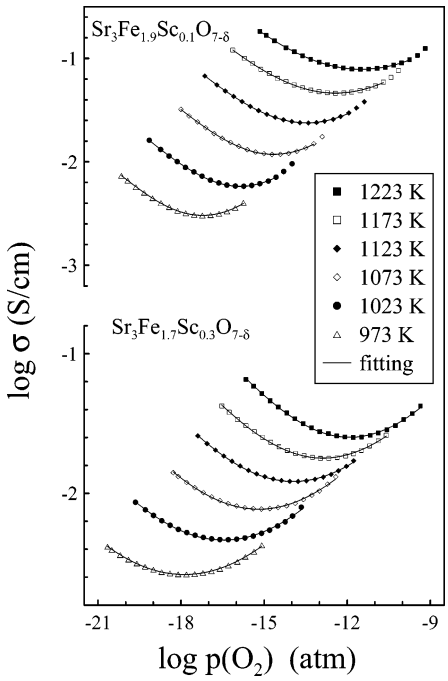

Figure 6. Oxygen partial pressure dependencies of the total conductivity of of $Sr_3(Fe,Sc)_2O_{7-\delta}$ in the vicinity of electron−hole equilibrium points. Solid lines show fitting results using eq 2 as regression model.

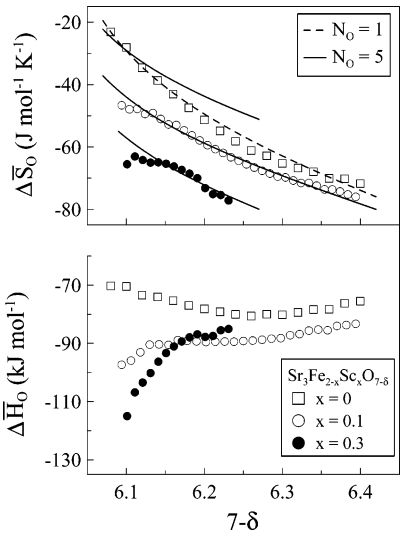

Figure 7. Partial molar entropy and enthalpy of oxygen, calculated from the nonstoichiometry data. Dashed and solid lines correspond to the ideal solution approximation, neglecting and accounting for the contribution of O3 sites, respectively.

the oxygen chemical potential variations with respect to a standard state in the gas phase

$$\Delta\mu_O(\delta,T) = \frac{1}{2}RT \ln p(O_2) \qquad (3)$$

Within the studied nonstoichiometry range, $\Delta\mu_o$ was found to depend linearly on temperature at δ = const. This makes it possible to calculate the partial molar enthalpy ($\Delta\bar{H}_O$) and entropy ($\Delta\bar{S}_O$) of oxygen in the RP phases

$$\Delta\mu_O(\delta,T) = \Delta\bar{H}_O(\delta) - T\Delta\bar{S}_O(\delta) \qquad (4)$$

The results are presented in Figure 7. The partial oxygen enthalpy in $Sr_3Fe_{2-x}Sc_xO_{7-\delta}$ (x = 0−0.1) is essentially independent of the vacancy concentration at δ < 0.85,

(25) Steinvik, S.; Norby, T.; Kofstad, P. In *Proceedings of the International Conference on Electroceramics IV;* Waser, R., Ed.; Verlag der Augustinus Buchhandlung: Aachen, Germany, 1994; Vol. 2, p 691.
(26) Mizusaki, J. *Solid State Ionics* **1992**, *52*, 79.
(27) Kofstad, P. *Nonstoichiometry, Diffusion, and Electrical Conductivity in Binary Metal Oxides*; Wiley-Interscience, New York, 1972.
(28) Chebotin, V. N. *Physical Chemistry of Solids*; Khimiya: Moscow, 1982; references therein.

Table 2. Calculated Energetic Effect for the Oxygen-Vacancy Formation in the O1 and O3 Sites with Respect to O2

composition	ΔE (eV)	
	O1 site	O3 site[a]
Sr_3Fe_{2O7}	−1.21	−1.19
$Sr_3Fe_2O_{6.5}$	−1.16	−0.96
$Sr_3Fe_{1.97}Sc_{0.03}O_{6.5}$	−1.16	−1.00
$Sr_3Fe_2O_6$		−2.56

[a] The data are averaged for six O3 positions marked in Figure 2B.

suggesting that the oxygen sites participating in the intercalation processes possess similar energetic parameters and, hence, the ideal solution approximation can be applied. As the p-type electronic change carriers are localized on iron cations,[6,7] the configurational entropy for oxygen incorporation reaction under oxidizing conditions is expressed as

$$\Delta S_O^{conf} = R\, ln\left(\frac{[V_O][Fe^{3+}]^2}{[O^{2-}][Fe^{4+}]^2}\right) \quad (5)$$

where $[V_O]$ is the vacancy concentration. Taking into account the electroneutrality condition for $Sr_3Fe_{2-x}Sc_xO_{7-\delta}$

$$\Delta S_O = R\, ln\left(\frac{\delta(2\delta - x)^2}{(N_O - \delta)(2 - 2\delta)^2}\right) + \Delta S_{Ox}^0 \quad (6)$$

where N_O is the number of oxygen sites involved in the oxidation reaction per unit formula, and the last term corresponds to the standard state. When all oxygen vacancies occupy the O1 sites, $N_O = 1$; if the O1 and O3 positions exhibit similar energetic affinity to vacancy location, $N_O = 5$. The $N_O = 1$ model provides a fairly adequate description of the partial oxygen entropy variations in undoped $Sr_3Fe_2O_{7-\delta}$ (Figure 7). For $Sr_3Fe_{2-x}Sc_xO_{7-\delta}$ ($x = 0.1-0.3$), the partial entropy changes at $\delta < 0.85$ can be described assuming that the O1 and O3 sites are both involved in the oxygen intercalation processes, as illustrated by the solid lines in Figure 7. These results confirm that Sc-doping indeed promotes disordering in the oxygen sublattice of $Sr_3Fe_2O_{7-\delta}$ at moderate levels of oxygen deficiency. When the nonstoichiometry increases, serious deviations from the ideal solution model are, however observed, probably because of a greater role of energetic nonequivalence between the oxygen sites surrounded by iron and scandium cations and/or progressive defect association. The former assumption is supported by the fact that the partial oxygen enthalpy at $\delta > 0.85$ tends to substantially lower values when x increases (Figure 7).

These hypotheses were further validated by the static lattice simulations. Table 2 summarizes the calculated energy variations corresponding to the formation of one oxygen vacancy in the O1 and O3 sites of undoped and Sc-containing $Sr_3Fe_2O_{7-\delta}$; the energy increments are given with respect to O2 positions in the same lattices. In all cases, the energetic affinity to vacancy location is maximum for the O1 sites, in agreement with literature data.[4,6,9,23] The formation of O3 vacancies is also favorable, but the corresponding energetic effects are lower than those for O1 sites, except for oxygen-stoichiometric $Sr_3Fe_2O_7$. However, the latter situation can only be considered as hypothetical; at elevated temperatures and ambient total pressure, the lattice of the RP strontium ferrite is always oxygen-deficient. Because the large difference in vacancy-formation energies for the O2 and O1/O3 positions (0.9−2.6 eV), the O2 site occupancy should be close to ideal.

Table 3. Calculated Energetic Effect for the Vacancy Formation in Selected Oxygen Sites of $Sr_3Fe_{1.97}Sc_{0.03}O_{6.5}$ Lattice with Respect to $Sr_3Fe_2O_{6.5}$

oxygen site	nearest B-site cations*		ΔE (eV)
	$Sr_3Fe_{1.97}Sc_{0.03}O_{6.5}$	$Sr_3Fe_2O_{6.5}$	
$O1_{173}$	Sc^{3+}(o), Fe^{3+}(o)	Fe^{3+} (o), Fe^{3+} (o)	0.19
$O2_{202}$	Sc^{3+}(o)	Fe^{3+}(o)	0.19
$O3_{363}$	Sc^{3+}(o), Fe^{4+}(o)	Fe^{3+}(o), Fe^{4+}(o)	0.29
$O3_{267}$	Sc^{3+}(o), Fe^{3+}(p)	Fe^{3+}(*o*), Fe^{3+}(p)	0.18
$O3_{268}$	Sc^{3+}(o), Fe^{4+}(p)	Fe^{3+}(o), Fe^{4+}(p)	0.21
$O3_{367}$	Sc^{3+}(o), Fe^{3+}(p)	Fe^{3+}(o), Fe^{3+}(p)	0.27
$O3_{263}$	Fe^{3+}(o), Fe^{3+}(o)	Fe^{3+}(o), Fe^{3+}(o)	0.00
$O3_{264}$	Fe^{4+}(o), Fe^{4+}(o)	Fe^{4+}(o), Fe^{4+}(o)	−0.02

[a] o and p correspond to octahedral and pyramidal coordination of the B-site cations prior to the oxygen-vacancy placement.

Table 3 lists the calculated vacancy-formation energy increments (ΔE) for various oxygen sites in $Sr_3Fe_{1.97}Sc_{0.03}O_{6.5}$ with respect to identical positions in $Sr_3Fe_2O_{6.5}$. When comparing the Sc-substituted and undoped ferrite lattices, one can conclude that the vacancy location near Sc^{3+} is energetically unfavorable with respect to Fe^{3+}; the corresponding energy difference varies in the range 0.18−0.29 eV. The vacancy formation energy in more distant oxygen sites, including the second coordination sphere, is essentially unaffected by scandium doping (cf. ΔE values for the $O3_{263}$ and $O3_{264}$ sites, Table 3). At a fixed nonstoichiometry, the resultant stabilization of ScO_6 octahedra should lead to increasing concentrations of occupied O1 and vacant O3 positions. This effect seems responsible for increasing disorder in the O1/O3 sites on doping, reflected by the ΔS_O variations.

3.3. Electronic Conduction. As for the parent strontium ferrite,[5−7] the total conductivity of $Sr_3Fe_{2-x}Sc_xO_{7-\delta}$ under oxidizing conditions is up to 1×10^2 to 1×10^3 times higher than that around the electron−hole equilibrium points and decreases with reducing $p(O_2)$, indicating that the electron−hole transport is predominant at high oxygen pressures (Figure 8). Because of the strong variations of the oxygen content with temperature (Figure 4), the conductivity has pseudometallic character typical for perovskite-related ferrites.[6,7,10,12−18] Another relevant tendency refers to decreasing σ values when Sc^{3+} concentration increases. Figure 9 illustrates the relationships between the total conductivity and oxygen content under oxidizing conditions. All these dependencies are nonlinear, displaying an increase of the hole mobility (μ_p) on decreasing δ. Such behavior originates from increasing concentration and covalency of Fe−O−Fe bonds responsible for the hole transport, when the oxygen content becomes higher and the lattice contracts. Obviously, doping with scandium has opposite effects.

The hole mobility (Figure 10) was estimated from data on the partial p-type electronic conductivity (σ_p) and oxygen nonstoichiometry, taking into account the electroneutrality condition

$$\sigma_p = epN_u\mu_p = 2eN_u\mu_p(1 - \delta) \quad (7)$$

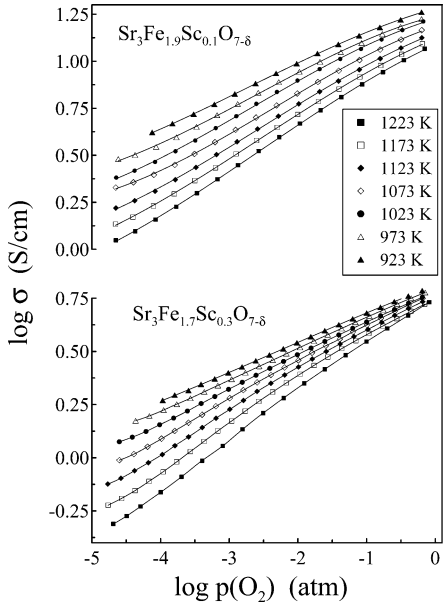

Figure 8. Oxygen partial pressure dependencies of the total conductivity of $Sr_3(Fe,Sc)_2O_{7-\delta}$ under oxidizing conditions. Solid lines are for visual guidance only.

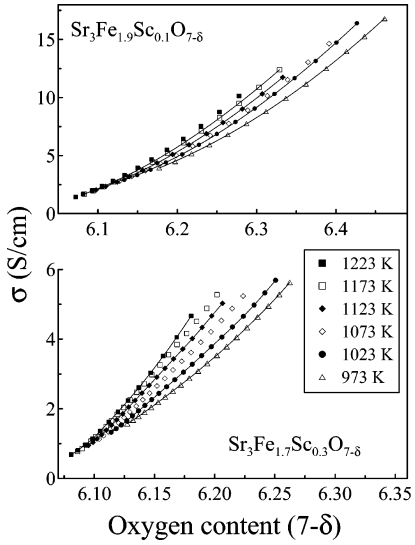

Figure 9. Total conductivity of $Sr_3Fe_{2-x}Sc_xO_{7-\delta}$ as function of the oxygen deficiency.

where p is the number of electron holes per unit formula (the presence of n-type electronic charge carriers under oxidizing conditions is neglected), N_u (cm^{-3}) is the volume concentration of formula units calculated from the structural data, and e is the elementary charge. The temperature-activated character of both hole mobility and conductivity (Figures 9 and 10) provides unambiguous evidence of a small-polaron mechanism, as for undoped $Sr_3Fe_2O_{7-\delta}$.[6,7] Accordingly, the μ_p values are below the accepted threshold of $\sim$0.1 $cm^2\ V^{-1}\ s^{-1}$, which is considered to separate small polaron and broadband conduction.[28,29] Hence, scandium additions appear to have no significant effect on the mechanism of p-type electronic transport, but lower the concentration and mobility of charge carriers, thereby decreasing conductivity.

(29) Goodenough, J. B.; Zhou, J.-S. In *Localized to Itinerant Electronic Transition in Perovskite Oxides*; Goodenough, J. B., Ed.; Springer-Verlag: Berlin, 2001; p 17 and references therein.

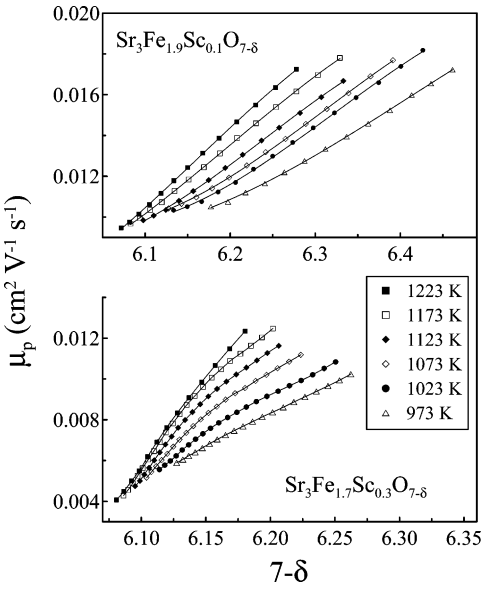

Figure 10. Hole mobility in $Sr_3Fe_{2-x}Sc_xO_{7-\delta}$ as a function of the oxygen content. Solid lines are for visual guidance only.

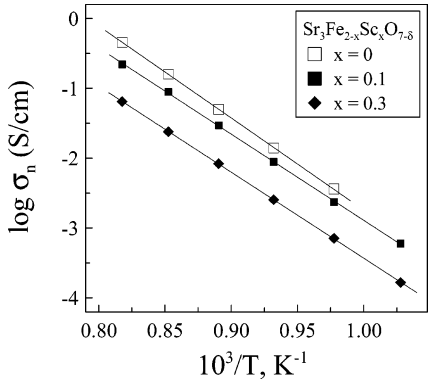

Figure 11. Temperature dependencies of the n-type electronic conductivity of $Sr_3Fe_{2-x}Sc_xO_{7-\delta}$ at $p(O_2) = 1 \times 10^{-16}$ atm.

A similar conclusion was drawn for the n-type electronic conduction. As an example, Figure 11 compares the temperature dependencies of partial n-type electronic conductivities (σ_n) of the $Sr_3Fe_{2-x}Sc_xO_{7-\delta}$ series at $p(O_2) = 1 \times 10^{-16}$ atm, calculated subtracting the oxygen-ion and hole contributions from total conductivity. The behavior in reducing conditions is similar to that observed in oxidizing atmospheres in that substitution of iron with scandium results in lower electronic transport. The activation energy for n-type electronic transport (E_n) exhibits a minor decrease when 5% Sc^{3+} cations are incorporated in the iron sublattice, but becomes essentially composition-independent on further doping, varying in the narrow range 2.46−2.54 eV at $x = 0.1-0.3$ (Figure 3). Notice that for perovskite-related ferrite materials, E_n correlates often with the phase decomposition enthalpy in reducing atmospheres, because these quantities are both determined by the iron−oxygen bonding energy.[6] One may expect, therefore, that the low-$p(O_2)$ stability limits of $Sr_3Fe_{2-x}Sc_xO_{7-\delta}$ should be similar for all studied compositions, although this hypothesis requires additional experimental verification.

3.4. Ionic Transport. Figure 12 presents the temperature dependencies of oxygen ionic conductivity in $Sr_3Fe_{2-x}Sc_xO_{7-\delta}$, calculated by eq 2. For undoped $Sr_3Fe_2O_{7-\delta}$, the Arrhenius

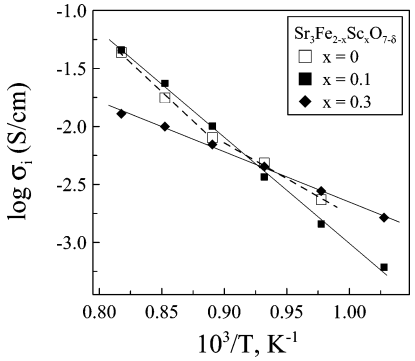

Figure 12. Oxygen ionic conductivity of $Sr_3Fe_{2-x}Sc_xO_{7-\delta}$ under reducing conditions.

plot displays a break at ~1120 K due to changing diffusion mechanism on heating.[6,9] In the low-temperature range, when the ion migration occurs mainly via the O3 → O1 → O3 jumps and is limited by the vacancy concentration in O3 sites, the apparent activation energy for ionic transport (E_i) is approximately 1.3 eV. At high temperatures when extensive disordering processes in the O3 sites start, the activation energy increases up to 2.0 eV at 1123−1223 K. These values are both in agreement with the calculated migration energies (E_m) in the undoped ferrite lattice, Tables 4 and 5. Note that because the energetic barriers for ion jumps between the energetically nonequivalent oxygen positions surrounded by different cations are asymmetric, the migration energies for both direct and reverse jumps are presented. For the mechanism involving O1 ↔ O3 jumps, the predicted E_m values vary in the range 0.90−1.43 eV, depending on the local environment of oxygen anions; the average migration energy is 1.2 eV. When migration occurs exclusively via the O3 positions, the energetic barrier is considerably higher, 1.54−2.18 eV (Table 5); the average E_m value is 1.8 eV. Notice that in the latter case, the apparent activation energy observed experimentally should also comprise a contribution associated with different vacancy-formation enthalpies in the O3 and O1 sites. On the basis of the computer simulation results (Table 2), this contribution can be estimated as ~0.2 eV. These trends correlate with shorter O3−Fe and O3−Sr bond distances with respect to the O1 sites[9] and reflect stronger cation−anion bonding for oxygen located in the O3 positions.

The substitution of scandium for iron suppresses the changes in anion diffusion mechanism on heating (Figure 12). The apparent activation energy for ionic transport in $Sr_3Fe_{2-x}Sc_xO_{7-\delta}$ becomes essentially temperature-independent at 973−1223 K and decreases with scandium additions down to 0.95 eV. Figure 3 compares the experimental E_i values for undoped strontium ferrite and Sc-substituted materials; in the case of $Sr_3Fe_2O_{7-\delta}$, the activation energy is given for the high-temperature range.

The computer simulations showed that oxygen anions in the first coordination sphere near Sc^{3+} are almost excluded from the diffusion processes, at least for the O1 positions (Table 4). The energy barrier for ion jumps involving O1 sites near Sc^{3+} is 0.21−0.72 eV higher than for the jumps near Fe^{3+} in the same defect configuration. For the O3 positions this difference is smaller, 0.08−0.22 eV (Table 5). However, these values should be considered only in combination with the energetic effects associated with oxygen vacancy location near Sc^{3+} with respect to Fe^{3+} (0.18−0.27 eV, Table 3). The incorporation of scandium into the $Sr_3Fe_2O_{7-\delta}$ structure hence leads to a lower concentration of mobile oxygen anions, but also increases the concentration of vacant O3 and O1 sites surrounded by iron. These vacancies, and the O^{2-} anions distant from Sc^{3+}, seem to provide a major contribution to the ionic conductivity. At the same time, a dominant role in oxygen migration processes can still be expected for the O1 → O3 → O1 pathways. Indeed, the apparent activation energies for ionic conduction in $Sr_3Fe_{2-x}Sc_xO_{7-\delta}$ ($x = 0.2-0.3$), 0.95−1.15 eV, are close enough to the calculated E_m values for anion jumps via the O1 and O3 sites surrounded by Fe^{3+} and Fe^{4+} cations in simulated $Sr_3Fe_2O_{6.5}$ lattice (Table 4).

Finally, whatever the microscopic diffusion mechanisms, the substitution of 15% iron cations with scandium makes it possible to increase oxygen ionic conductivity of the RP type strontium ferrite at temperatures below 1000 K (Figure 12). Another positive effect is related to decreasing oxygen nonstoichiometry variations (Figure 4), which should provide

Table 4. Calculated Oxygen-Ion Migration Energies for the O1−O3 Pathways in $Sr_3(Fe,Sc)_2O_{6.5}$

	initial ion position		final ion position		
composition	oxygen site	nearest B-site cations	oxygen site	nearest B-site cations	E_m (eV) (direct/reverse jump direction)
$Sr_3Fe_2O_{6.5}$	$O1_{173}$	Fe^{3+}, Fe^{3+}	$O3_{367}$	Fe^{3+}, Fe^{3+}	1.28/0.90
	$O1_{173}$	Fe^{3+}, Fe^{3+}	$O3_{363}$	Fe^{3+}, Fe^{4+}	1.30/1.20
	$O1_{173}$	Fe^{3+}, Fe^{3+}	$O3_{268}$	Fe^{3+}, Fe^{4+}	1.43/1.40
	$O1_{173}$	Fe^{3+}, Fe^{3+}	$O3_{267}$	Fe^{3+}, Fe^{3+}	1.10/1.13
$Sr_3Fe_{1.97}Sc_{0.03}O_{6.5}$	$O1_{173}$	Sc^{3+}, Fe^{3+}	$O3_{367}$	Sc^{3+}, Fe^{3+}	1.58/1.12
	$O1_{173}$	Sc^{3+}, Fe^{3+}	$O3_{363}$	Sc^{3+}, Fe^{4+}	1.64/1.44
	$O1_{173}$	Sc^{3+}, Fe^{3+}	$O3_{268}$	Sc^{3+}, Fe^{4+}	1.64/1.59
	$O1_{173}$	Sc^{3+}, Fe^{3+}	$O3_{267}$	Sc^{3+}, Fe^{3+}	1.33/1.37

Table 5. Calculated Oxygen-Ion Migration Energies for the O3−O3 Diffusion Pathways in $Sr_3(Fe,Sc)_2O_{6.5}$

	initial ion position		final ion position		
composition	oxygen site	nearest B-site cations	oxygen site	nearest B-site cations	E_m (eV) (direct/reverse jump direction)
$Sr_3Fe_2O_{6.5}$	$O3_{367}$	Fe^{3+}, Fe^{3+}	$O3_{268}$	Fe^{3+}, Fe^{4+}	1.83/2.18
	$O3_{268}$	Fe^{3+}, Fe^{4+}	$O3_{363}$	Fe^{3+}, Fe^{4+}	1.84/1.77
	$O3_{363}$	Fe^{3+}, Fe^{4+}	$O3_{267}$	Fe^{3+}, Fe^{3+}	1.54/1.67
$Sr_3Fe_{1.97}Sc_{0.03}O_{6.5}$	$O3_{367}$	Sc^{3+}, Fe^{3+}	$O3_{268}$	Sc^{3+}, Fe^{4+}	1.95/2.36
	$O3_{268}$	Sc^{3+}, Fe^{4+}	$O3_{363}$	Sc^{3+}, Fe^{4+}	2.00/1.85
	$O3_{363}$	Sc^{3+}, Fe^{4+}	$O3_{267}$	Sc^{3+}, Fe^{3+}	1.65/1.89

a lower chemically induced expansion and thus improved thermomechanical stability of dense $Sr_3(Fe,Sc)_2O_{7-\delta}$ ceramics. Taking into account that $Sr_3Fe_2O_{7-\delta}$ has superior thermodynamic stability at low oxygen chemical potentials in comparison with other mixed-conducting phases in the ternary Sr−Fe−O system,[6] these effects may be of interest for developments of novel membrane materials. On the other hand, further experimental work is necessary to evaluate the stability of $Sr_3Fe_2O_7$-based solid solutions in atmospheres with high partial pressures of carbon dioxide, water vapor and/or sulfur oxides. The relatively high strontium activity in $Sr_3(Fe,Sc)_2O_{7-\delta}$ may lead to fast surface poisoning due to interaction with these gases. Additional studies are also necessary to assess possible protonic contribution to the total conductivity at intermediate temperatures, caused by water intercalation into the rock-salt layers of $Sr_3Fe_2O_7$-based structure,[30] and hydration effects on the electronic transport.

4. Conclusions

The solubility of scandium cations in the Ruddlesden−Popper type lattice of $Sr_3Fe_{2-x}Sc_xO_{7-\delta}$ corresponds to approximately 16−18% of the iron site density. The incorporation of Sc^{3+} increases tetragonal unit-cell volume and oxygen nonstoichiometry and decreases partial p- and n-type electronic conductivities in the oxygen partial pressure range from 1×10^{-20} to 0.7 atm at 973−1223 K. The relatively low, temperature-activated hole mobility indicates that the electronic charge carriers are localized on iron cations. If compared to undoped $Sr_3Fe_2O_{7-\delta}$, no essential alterations in the electronic transport mechanisms are observed. At the same time, doping with scandium promotes oxygen-vacancy disordering in the perovskite-type layers of $Sr_3(Fe,Sc)_2O_{7-\delta}$ structure because of the formation of stable ScO_6 octahedra, confirmed by atomistic modeling. This leads to changing occupancies of the apical O1 sites linking iron−oxygen polyhedra along the *c*-axis, and equatorial O3 positions in the perovskite-type planes. The computer simulations showed that ScO_6 octahedra are essentially excluded from the ionic transport processes. A key contribution to oxygen ion diffusion is expected for pathways involving the O1 and O3 sites surrounded by iron, which are characterized with substantially lower migration energy if compared to direct O3 → O3 jumps. Increasing concentration of vacant O3 sites, induced by Sc^{3+} doping, results in a monotonous decrease in the ionic transport activation energy, whereas the partial ionic conductivity of $Sr_3Fe_{1.7}Sc_{0.3}O_{7-\delta}$ becomes higher than that of undoped $Sr_3Fe_2O_{7-\delta}$ at temperatures below 1000 K.

Acknowledgment. This work was partially supported by the Russian Foundation for Basic Research (grant 06-03-33099), by the FCT, Portugal (project POCI/CTM/58570/2004), and by the Ural Division of Russian Academy of Sciences (contract 7-1-K).

CM071364U

(30) Matvejeff, M.; Lehtimaki, M.; Hirasa, A.; Huang, Y.-H.; Yamauchi, H.; Karppinen, M. *Chem. Mater.* **2005**, *17*, 2775.